Research Square

Preprints are preliminary reports that have not undergone peer review.
They should not be considered conclusive, used to inform clinical practice,
or referenced by the media as validated information.

Comparative study of the compatibility of aliphatic polyketone tercopolymer blends using a technique combining scanning electron microscopy and energy-dispersive X-ray spectroscopy.

Shichoon Lee

tonygren@jwu.ac.kr

Jungwon University https://orcid.org/0000-0002-2289-8734

Research Article

Keywords: compatibility, polyketone, Nylon 6 (polyamide 6), styrene-acrylonitrile(SAN), polymer blend, morphology, SEM/EDS elemental mapping, SEM/EDS elemental line scanning, interfacial thickness

Posted Date: June 30th, 2026

DOI: https://doi.org/10.21203/rs.3.rs-10033532/v1

License: This work is licensed under a Creative Commons Attribution 4.0 International License.
Read Full License

Abstract

The compatibility of polyketone (PK)/polyamide6 (PA) and PK/styrene-acrylonitrile (SAN) polymer blends was compared through elemental analysis combining scanning electron microscopy (SEM) and energy-dispersive X-ray spectroscopy (EDS). Elemental mapping technology reveals sea and island-like phase separation patterns more clearly than SEM observations, as well as the continuous domain-in-domain form of PK/SAN and the layered structure of PK/SAN/additive mixtures. The SEM/EDS elemental mapping results for the PK/PA mixture showed no overall phase separation; instead, nanoscale separation structures similar to those observed by transmission electron microscopy (TEM) were clearly visible, proving that this is a useful method for evaluating the compatibility of polymer blends. Elemental line scan results for the PK/SAN blend showed a significant gradient in the intensity of oxygen and nitrogen elements across the interface, indicating a large compositional difference between the two phases and a lack of compatibility. The interfacial thickness of the PK/SAN blend, estimated using the compositional gradient observed in the line scan, was approximately 0.17–0.51 μm. It was found that the interface thickness of the PK70/PA30 blend was ranged 0.3 to 0.7 μm, that of the PK30/PA70 blend showed no significant compositional differences in nitrogen and oxygen pulse intensities across the interface, suggesting active interdiffusion, adhesion, and a thich interface and that the interface of the PK30/PA70 blend is too thick to be estimated using this line scanning technique. Both elemental mapping and line scanning techniques clearly demonstrate that the PK polymer blends better mixed with the PA polymer than with the SAN polymer, suggesting that the PK/PA blend possesses superior compatibility. These observations indicate that a method combining SEM morphological observation with EDS elemental mapping and line scanning can serve as a more advanced approach for quantitatively evaluating the compatibility of polymer blends.

1. Introduction

In polymer blends, miscibility between constituent components affects mechanical properties, thermal property, optical property, and electrical properties for polymer blend [1, 2]. Each property of a miscible blend generally tends to be slightly higher or lower than sum of the value of the volume ratios of the respective property value of constituent component. Although a polymer blend is not mixed on a molecular scale, if it doesn't separate in a gross scale and has a certain degree of miscibility and good adhesion at the interface, it is said to be compatible polymer blend whose properties are complementary [1, 2]. Even some immiscible polymer blend gives desirable or beneficial properties than the value corresponding to the volume ratio of the properties of each component, so it can be said that the polymer blend has partial miscibility and some extent of compatibility.

There are several methods to evaluate the miscibility of polymer blends are known, such as glass transition temperature (Tg) transition, dynamic mechanical property change, dielectric constant change, calorimetry, light scattering method, morphological observation, and observation of transparency change. The physical/mechanical properties of polymer blends, such as tensile strength, impact resistance and modulus are closely related to the controlled morphology, and how much homogeneous

the morphology is. Thus, morphological observation is a good tool to investigate the presence of phase separation and evaluate miscibility of polymer blend [2]. In a miscible blend, each phase is so well-mixed that is difficult to distinguish phase boundary. In an immiscible blend, the separated phase can be clearly noticeable, its domain size is measurable, and voids and detachments at the interface can be observed.

Miscible polymer blend has good compatibility; however, the miscible pair is rare case in polymer blend [1, 2]. Miscibility in polymer blends not basic requirement for providing applicable properties. Even in an immiscible blend, there is a certain degree of miscibility so that the respective Tg of each phase shifts inward. It has been reported that in the dynamic mechanical test for PK/PA blend, the tan delta value can also be seen to shift to the middle [3, 4, 5]. This is interpreted as one polymer dissolving into the other to some extent. Depending on the degree of mixing, the transition of Tg appear to vary [4, 5]. If two polymers is distributed uniformly on a molecular scale [2], it will not exhibit any separated phase and show single Tg. However in each phase of the immiscible polymer blend, one polymer doesn't distribute evenly and completely mixed with the other. Each phase in the immiscible blend is composed of major and minor polymer constituents. The compositional difference in each phase creates a contrast of image where the separated phase appeared and the phase morphology is developed [5, 6]. There is no standard for how much compositional difference in polymer phase creates the phase morphology. As miscibility increases, compositional difference weakens so that the phase morphology should become finer and the contrast becomes diminished.

Scanning electron microscopy (SEM) is one of the direct tools to determine whether a blend is miscible or immiscible. In immiscible polymer blends, SEM observation provides not only the separated domain but also the adhesion characteristics at the interface. However, SEM observation leaves ambiguity due to uncertain interfaces and confuses the determination of domain size. To accurately observe the morphology, the sample must be prepared in a detailed and skillful manner. For example, it must be fractured evenly in a liquid nitrogen atmosphere to avoid artifacts due to craze and yield deformation along the newly formed surface upon fracture [6]. Sometimes the etching of domain enhanced the contrast of phase morphology. However, care must be taken when selecting an etchant; it must be a non-solvent for the matrix and a good solvent for the domain phase.[6, 7, 8] To prepare polymer specimens for TEM observation, they must be cut under cryogenic conditions to avoid undesirable deformation. These procedures are so tedious and cumbersome that it is difficult to make them thin enough to observe the microstructure. In particular, staining is limited today by the use of hazardous chemicals [2, 9].

Aliphatic polyketone (PK) is an alternating copolymer produced using α-olefin monomers such as ethylene, propylene, and carbon monoxide, and those are commercially available and less expensive polymeric materials and production of PK potentially contribute to reducing carbon in the atmosphere [11–15]. Because the mechanical, thermal, and chemical resistance of PK is as high as that of some engineering plastics, PK has promising potential to replace some expensive engineering plastics [10–11]. However, melt processing of PK is mostly accompanied by gelation, crosslinking, and decomposition, and these disadvantages limit the processing range and application fields [16–19].

Copolymerization and polymer blending are useful ways to challenge processing problems. Generally, copolymerization introducing 6 mol% of propylene monomer as a third monomer lowers the melting point (Tm) and reduces heat resistance, but expands the processing range and application fields [20, 21].

Some alternating propylene-carbon monoxide copolymer (P-CO) have been reported to be miscible with blending of poly(methyl methacrylate, PMMA)[22] and poly(styrene-r-acrylonitrile, SAN)[23] in all compositions. When PK (including a terpolymer containing 6 mol% propylene monomer) is melt-mixed with other polymers, an immiscible blend is generally produced. For an immiscible polymer blend to have applications, it must have high compatibility. Marklund et al. [24] studied a PK/maleate polypropylene (PP) blend, which is an immiscible blend, and found that the addition of an additive with a diamine functional group improved interfacial adhesion, reduced domain size, and improved oxygen barrier properties. The Asano research group discovered that PK/PA blends prepared under high humidity conditions exhibit high impact characteristics and that the glass transition temperature (Tg) shifted inward in dynamic mechanical thermal analysis, suggesting partial miscibility of the blend [3, 4]. Lee et al. investigated compatibility of PK/SAN [6] and PK/PA blends [5] by experimental characterization including DMTA analyses and morphological observation of the fractured surface and the etched surface using SEM. The blend of PK/amorphous PA (Zytel330) revealed an enhanced mechanical property even when adding small amount (about 0.5%) of the blended component of PK with graphene-grafted PA as a compatibilizer [25]. The PK/rubber blend with high impact strength has been obtained in which PA formed an interphase in the PK/rubber blend and act as a compatibilizer [9].

Elemental analysis and mapping using scanning electron microscopy (SEM) and transmission electron microscopy (TEM) combined with energy-dispersive X-ray spectroscopy (EDS) is used to characterize the elemental distributions in minerals [26] and biomaterials [27], nanostructured materials,[28] and quantum dots [29] as well as polymer blend [30]. By performing phase identification and interfacial region of a ternary polymer blend consisting of polybutylene succinate (PBS), polylactic acid (PLA), and polycaprolactone (PCL) using compositional and elemental mapping analysis using time-of-flight secondary ion mass spectrometry (ToF-SIMS), and the interfacial thickness was quantitatively measured across the two interfaces (PLA/PBS and PLA/PCL) [31]. The technique provides enhanced microscopic analysis techniques in addition to morphological observations of polymer blends.

In this study, PK/SAN and PK/PA blends were manufactured and their compatibility was assessed through elemental analysis and mapping using a combined SEM/EDS technique. The elemental distribution varies depending on the composition of the polymers constituting each phase. EDS line scanning along the interface quantifies the distribution of each element, and visualizing elemental changes across the interface allows for the estimation of the interfacial thickness of the blend. Measuring the interfacial thickness can be a valuable method for assessing the compatibility of polymer blends.

2. Materials and Methods

2.1. Materials

PK is a terpolymer with an ethylene/propylene molar ratio of 96/4, grade M930A purchased from Hyosung Coporation, with a weight-average molecular weight (Mw): 132,000 g/mol, polydispersity: 2.2, melt flow rate (MFR): 170 dg/min at 2.16 kgf and 240°C. Poly(styrene-*random*-acrylonitrile) is grade SAN320 purchased from Kumho Petrochemical Co., with an acrylonitrile content of 40 mol%, Mw: 104,000 g/mol, MFR: 36 dg/min at 2.16 kgf and 240°C. PA(Nylon 6) is grade TK2451 with an Mw of 34,000 g/mol purchased from Taekwang Chemical Co., in South Korea.

2.2. Preparation of testing specimens

The specimens for morphological observations were prepared by melting and mixing PK and PA polymers using an LG Machinery injection molding machine and then injection molding. The test specimens were produced using an ASTM-family mold. The nozzle temperature of the injection molding machine was 240°C. The cycle time for injection molding was 1 minute.

2.3. Scanning Electron Microscopy (SEM) and Energy Dispersive X-ray Spectroscopy (EDS)

For SEM/EDS analysis, the central portion of the tensile specimen was taken. In particular, to prevent deformation structures at the interface, low-temperature fracture treatment was performed under a liquid nitrogen atmosphere. After coating the specimen surface with gold, SEM/EDS analysis was performed on the flow cross-section and flow plane. Low-temperature fracture surfaces were observed at low acceleration voltages of 5–10 kV to reduce the interaction volume caused by the electron beam using a field emission SEM of the Tescan Magna model equipped with a Schottky-cooled field emission electron gun (FEG), and EDS mapping images for the elements C, O, and N were obtained in the same SEM plane using a Bruker F model and an XFlash 6-100 detector.

2.4. Transmission Electron Microscopy (TEM)

Transmission electron microscopy images were taken using a field emission transmission electron microscope (JEM-2100F) from Jeol Ltd., with the electron beam accelerating voltage set to 200 kV. The micro-dissected samples were pretreated with phosphotungstic acid (PTA) [3, 4] and then immersed in an osmotic acid (OsO_4) solution [9].

3. Results and discussion

3.1. Morphological observations with elemental mapping

Morphological observation is considered a direct method for determining the compatibility of polymer blends. In immiscible blends, distinct domains are observed, and the blends exhibit phase separation and low interfacial adhesion. Increased compatibility induces interfacial interdiffusion and interactions

between the components. In immiscible blends, the increase in interdiffusion and interactions decreases domain size [1, 2].

Figure 1 shows morphological observations of PK70/SAN30 blend using SEM coupled with EDS (SEM/EDS) elemental mapping. Elemental characterization and mapping were performed for C, O, and N elements directly following by SEM observations. The detected and measured elements were mapped onto the same SEM photographs. SEM/EDS elemental mapped images show better contrast between matrix and domain phase rather than SEM image [6]. Among the images for each element, the image mapped for oxygen element is clearer than the images mapped for C, N, and all constituent elements. This is because of no content of oxygen in the SAN chain but high percentage of oxygen atom is present in the PK repeating unit.

Figure 2 shows the SEM image of the PK30/SAN70 blend, in which SAN is the main component, and the elemental mapping on the same image. Although the interface is not clearly visible in the SEM image of the SAN matrix blend, it can be identified more clearly through EDS mapping. In particular, as can be seen in Fig. 2b, the EDS mapping for the oxygen element appears much sharper than the mapping for other elements. However, upon closer examination, unlike the PK70/SAN30 blend where the PK phase is the matrix, the interface on the SAN matrix in the PK30/SAN70 blend appears blurry, and most of the dispersed domains appear coarse rather than spherical. This suggests that a continuous phase in which both PK and SAN are the matrix has been formed, or that a coarse phase has been formed due to the fusion of domains. Since the viscosity of PK is lower than that of SAN at an injection temperature of 240°C [2, 5, 6], it is highly likely that a continuous phase will form in the PK30/SAN70 composition even when PK is a minor component.

Figure 3 shows the PK70/PA30 blend, but interface between the matrix and a dispersed phase is unclear. PK/PA blend has been reported to be immiscible [7, 8] and partially miscible [3, 4, 5] due to their excellent mechanical properties resulting from fine domain morphology and strong interfacial adhesion at the interface. As shown in the SEM/EDS elemental mapping in Fig. 3, the interface is difficult to clearly identify. This is because the average domain size is on the submicron scale, indicating that the dispersed phase is well dispersed and diffused in the matrix phase vice versa, making it difficult to distinguish the interface.

Figure 4 shows the morphological observations of the PK30/PA70 blend, but it is difficult to clearly distinguish the interface between the matrix phase and the dispersion domains in the figure. SEM/EDS mapping for C, O, and N elements (Fig. 4b) reveals a yellow, narrow valley-shaped network structure surrounding the principal component, indicating a phase rich in the minor component PK, suggesting that the major component is a PA-rich phase. The nitrogen element mapping in Fig. 4d shows a thin, connected phase. Narrow, dark valley-shaped regions parallel to the nitrogen-rich PA phase represent PK phase with low nitrogen. As the compositional difference between the two phases decreases, dispersed domains with finer particle forms appear, making the interface even more indistinct. This image

demonstrates that the minor component PK exhibits a continuous form within the matrix phase without typical spherical domains.

This morphology was not visible when observing fracture surfaces or etched surfaces using SEM. [5, 7, 8, 9] EDS elemental mapping results clearly demonstrate that the PK polymer mixes better with the PA polymer than with the SAN polymer, suggesting that the PK/PA blend exhibits high compatibility without gross phase separation. These observations indicate that combining SEM morphological observations with EDS mapping can be a more advanced method for evaluating the compatibility of polymer blends.

3.2. TEM observation

The morphological observation with TEM can be used as a visual criterion for determining [1, 2, 3, 4, 9] whether the SEM/EDS elemental mapping technique investigated in this study is suitable for observing the compatibility of polymer blends. In practice, producing specimens suitable for TEM requires several cumbersome procedures and tasks, such as skilled microtome processing, epoxy molding, and staining with hazardous chemicals, limiting its practicality. Therefore, if SEM/EDS elemental analysis could evaluate compatibility as effectively as TEM observation, it would be a convenient and alternative tool. In this study, a two-step staining method using PTA and OsO_4 reagents was carried out to enhance the contrast of the PA domains. As shown in Supporting Information Figure S1, the contrast of the domains was enhanced. The TEM image of the PK70/SAN30 blend shows that the dispersed SAN domains are over 1 μm in size, which is approximately the same size as observed in the SEM observation.

The PA-rich domains dispersed in the PK70/PA30 blend are submicron in size. The interfaces of blend are indistinct, indicating high interfacial diffusion and adhesion. In the PK30/PA70 composition, despite the low PK content, the PK phase maintains an interconnected structure with the PA phase. This co-continuous structure forms thin valleys that are connected in a layered form, with the PK phase surrounding the PA phase. Although this observation that a valley-shaped network structure is formed despite a small amount of PK was not confirmed in the SEM images, it is consistent with the SEM/EDS elemental mapping images a shown in Fig. 4.

TEM observations revealed clearer images, especially for the PK/PA blend, and its domain sizes were clearly observed even at the submicron scale. The size of the dispersed domain (domain size) is related to the interfacial tension between the phases that constitute the matrix and dispersed domains in the polymer blend. The lower the interfacial tension in the polymer blend, the greater the inter-diffusion between the phases, resulting in a thick interface and a fine dispersed domain size [32]. Such high diffusion and compatibility in PK/PA blends can be explained by the high interaction resulting from hydrogen bonding between the amide group of PA and carbonyl group of PK [25, 33]. We found that the morphology of the PK/PA blend is much finer. From a comparative morphological study, PK/PA blend has a lower interfacial tension and a higher interaction than that of PK/SAN blend. This is because the two polymers, PK and PA, have high compatibility, even though PK and PA are an immisible.

However, it has been reported that PK/PA blend has as high mechanical properties as compatible blend. [3, 4, 5] The Izod impact strength of PK/PA polymer blend is higher than that of the linear mixing law at all blend compositions [3, 4, 5, 7, 8] An improvement in impact strength requires not only good interfacial adhesion and prevention of coalescence [1, 2, 5, 9] but also appropriately larger domain size that could toughen the matrix phase. It is known that domain sizes larger than the critical size are necessary to toughen blends [9, 34, 35]. The smaller dispersed domain sizes resulting from high compatibility and low interfacial tension do not always provide improved impact properties. The fact that PK/PA blend exhibits high impact strength with a small domain size of less than 200 nm suggests that interfacial reactions occurred at the interface of the PK/PA mixture, leading to increased interfacial adhesion.

Son et al. [7, 8] investigated the compatibility and chemical reactions between aliphatic polyketone (PK) and polyamide 6 when melt-mixing end-capped polyamide 6 and aliphatic polyketone (PK) in an intensive mixer. No increase in mixing torque was observed in the melt-mixing using end-capped polyamide 6, but the mixing torque increased significantly in the melt-mixing using polyamide6 with primary amine end group. Additionally, FT-IR analysis confirmed that polyamide functional groups were present only in the melt-mixed and solvent-extracted samples of polyamide 6 with primary amine end groups and PK. This study suggests that amine-end groups are involved in chemical reactions, and that the copolymer formed by these reactions refines the dispersion region.

It is well known that intermolecular and intramolecular aldol condensation reactions of polyketones (PK) at high temperatures induce crosslinking reactions [16, 17, 18]. Therefore, an increase in mixing torque occurs not only through copolymer formation but also through crosslinking and decomposition [7, 8]. This leads to an increase in melt viscosity and mixing torque. An increase in amine groups suggests that both crosslinking and copolymerization reactions are enhanced. It is presumed that the nucleophilicity of the anionic components of PA, such as primary amine end groups, promotes crosslinking reactions during melt processing of PK and mixtures thereof. Additionally, an increase in amine end group promotes the reaction between amine groups and carbonyl groups to form copolymers [8].

It has been reported that in immiscible blends, the conversion of coupling reaction between functional groups is much less than that in miscible blends, making it difficult to quantify the degree of reaction at the interface using analytical methods [36, 37, 38]. However, it is known that even such a low degree of interfacial reaction significantly influences the determination of the blend's morphology and mechanical properties. By crosslinking reaction and gelation of PK and PA, impact strength would be increased but not provide finer morphology. The copolymer formed by this chemical reaction reduces domain size and improves interfacial adhesion. This reactive compatibilization enhances mechanical properties, such as tensile and impact characteristics.

3.3. Elemental mapping for additive modified PK/SAN blends

Morphological changes in the PK/SAN blend were observed using SEM/EDS elemental mapping when ethylene glycidyl methacrylate (EGMA) terpolymers were added. When well-designed compatibilizers or

surface active agent are added, they are positioned at the interface between the two phases, thereby lowering surface tension. Low surface tension induces high interfacial diffusion and entanglement, which reduces the domain size of the dispersed phase and makes the shape of the dispersed phase finer [2]. Immiscible polymers can be compatibilized through reactions between functional groups present in each polymer during processing, and this reactive compatibilization is known to be effective for the compatibilization of immiscible polymers [32, 36–39].

When EGMA is added to the PK70/SAN30 blend, it is known that the oxirane ring of EGMA reacts with the hydroxyl group of β-hydroxyketone [40–43] by aldol reaction of PK [18], but it also appears to interact intermolecularly with the cyano group of the SAN chain. As can be seen in Figs. 6a and 6b, the dispersed SAN phase is spherical, which is somewhat finer than when EGMA was not added (see Figs. 1a, 1b and Supplementary Figure S2). Thus, significant morphological refinement was not observed, suggesting that the EGMA added as a compatibilizer did not induce reactive compatibilization at the interface but merely refined the shape of the blend through intermolecular interactions [44].

In contrast, in compositions where SAN is the matrix, a continuous form linked to the PK phase was observed, as can be seen in Figs. 6c and 6d, which was not observed in compositions without EGMA added, as can be seen in Fig. 2. Additionally, a domain-in-domain form in which SAN domains exist within the dispersed PK phase can be observed in the microstructure. S. Li et al. [45] reported that when PK is greater than 40 vol.%, the PA12 phase exists in a nanostructured form within the PK domains in PK/PA12 blends, which is attributed to hydrogen bonding between PK and PA12 and contributes to the improvement of high mechanical properties. Identifying the interfacial location of the additive is important for evaluating its performance as a compatibilizer. EGMA appears to be preferentially present on the PK rather than at the interface, because of considering the structure of the EGMA polymer with a polyethylene backbone. By increasing resolution and selecting an appropriate pair of polymers, the location of the compatibilizer can be observed using SEM/EDS elemental mapping.

The morphology observed in the direction of melt flow clearly shows a layered structure in which a thick SAN phase is stacked next to a thin PK phase (Figs. 6e and 6f). Layered nanostructures are receiving significant attention in the field of polymer composites due to characteristic enhancements in mechanical strength, thermal properties, barrier properties, and flame retardancy [44–46]. Morphological advancements that create micro-separated stacked structures with layers approximately 200 nm thick, rather than nano-separated structures, influence the properties of the blend. While this type of stacked structure and domain-in-domain morphology cannot be observed with SEM alone, they can be clearly observed using SEM/EDS elemental mapping techniques.

3.4. Interfacial thickness estimation using EDS line scanning mode

As shown in Fig. 7, the line scanning mode of elemental analysis demonstrates the potential to quantitatively measure constituent elements along the intersection lines of the polymer blend. Pulse intensity is related to the number of detected elements and is displayed along the scan line. In the PK

matrix phase of Fig. 7a (PK70/SAN30 blend), oxygen intensity is high but decreases as it passes the interface. The pulse intensity of the oxygen element gradually decreases and converges to a low flat value in the SAN-rich region. As the scan passes this region and approaches the opposite interface, the oxygen pulse intensity increases back to its original value. The line scan of the nitrogen element moves in the opposite pattern to that of the oxygen element. Nitrogen intensity tends to increase as it passes through the SAN domain, maintains high intensity along the dispersed SAN domain, and then tends to decrease as it moves out of the dispersed domain phase.

The interface thickness can be estimated from the abrupt changes in the intensity profile slopes of O and N elements. However, due to the variability of the measured pulse intensity values of oxygen and nitrogen, it is difficult to establish background values for each element within the matrix and domain. As shown in Fig. 7a and Table S1 (Supplementary Information), the matrix and domain were divided left and right based on the SAN domain boundary observed in the SEM image, and their respective background values were calculated. The intensities of at least 15 pulse points in each background region of the SAN domain boundary were averaged, and the standard deviation was calculated. The background values for each matrix and domain were calculated to be 168 and 84, respectively, with a standard deviation of 8.2 or less. The interface thickness was estimated based on the background values between each region; specifically, it is determined by calculating the scan distance from the point where the background line of each region intersects with the region where the pulse intensity rapidly increases or decreases around the vertical dashed line (observed as the domain boundary in the SEM image of Fig. 7a).

It is known that in EDS analysis, the electron beam induces interaction regions within the sample, causing pulse intensity to tend to gradually increase or decrease, which leads to reduced measurement reliability. Due to the low density of polymer materials, the interaction volume of the electron beam within the sample reaches several micrometers when an acceleration voltage is applied; consequently, a beam broadening effect occurs during EDS analysis, where the interface signal spreads more widely than it actually does. Therefore, data with gradual changes in pulse intensity at the interface and high variability were not considered meaningful. The pulse intensity was normalized to set the values in the PK matrix and SAN domain to 1 and 0, respectively. This allowed us to locate scan distance positions corresponding to 16% and 84% of the background value [49, 51]. When these two locations were estimated as the interface, the difference was 0.44 μm for element O. For element N, the interface thickness calculated using the same procedure was 0.31 μm. However, the matrix background value for O and N element (rightside background) could not be determined because the pulse intensity continuously fluctuated as it passed through the SAN domain and re-entered the PK matrix as shown in Fig. 7a and Table S1,

As shown in Fig. 7b, the PK30/SAN70 blend is composed primarily of SAN components and exhibits a continuous structure in which the SAN phase exists within the dispersed PK domain. A line scan can be observed starting from the left side of the image (i.e., the SAN phase), passing through a narrow PK region, re-entering the SAN phase sandwiched between them, and then sequentially passing through another narrow PK region and the SAN phase. It can be seen that four interfaces exist along the line

scan. In the narrow PK region, the oxygen pulse intensity increases sharply, exhibiting a peak-shaped intensity graph. Conversely, in the SAN region sandwiched between the PK-rich phases, the oxygen intensity graph shows a downward convex shape. Additionally, the peak-shaped pulse intensity reappears when the scan passes through another narrow PK phase. In this measurement, no graph noise patterns showing gradual increase and decrease due to interaction volume were observed. It can be said that this is a more reliable measurement of interface thickness. As can be seen in Fig. 7b, the line scan shape of nitrogen atoms generally moves in the opposite direction to that of oxygen atoms. Furthermore, this graph shape is inverse of the corresponding line scan pattern of the PK70/SAN30 blend of Fig. 7a. The background value for the O element in the PK30/SAN70 blend was set as the peak value of the PK domain, and in the SAN matrix, it was set in the same way as above stated. Additionally, the end of the interface was defined as the point where it decreases abruptly monotonically and meets the background line on the SAN domain (see Fig. 7b and Table S1). Based on oxygen element, the four interface thicknesses were estimated to be 0.48 μm and 0.51 μm, and 0.41 μm and 0.17 μm, respectively. (Fig. 7b and Table S1)

Although the interface was indistinct in SEM observations of the PK70/PA30 blend, line scanning results of oxygen atoms showed a downward convex pattern along the PA dispersion region after passing through the interface. In contrast to oxygen atoms, line scanning of nitrogen atoms exhibited an upward convex shape, as shown in Fig. 7c. The intensity gradient at the interface appeared gentler than that of the PK/SAN blend, and it was difficult to draw a baseline within the domain region; this indicates continuous compositional change and may be related to the thick interface thickness. In fact, the estimated thickness of the first interface scanned on the left was 0.76 μm for O and 0.37 μm for the element (Fig. 7c and Table S1). The second interface on the right could not be measured because it was difficult to set the background value.

Line scanning results of the PK30/PA70 blend, in which PA is the main component, showed no distinct interface, and there was no significant difference in nitrogen and oxygen pulse intensities across the interface. Therefore, it was impossible to determine the location of the interface or estimate its thickness (see Fig. 7d). This suggests that the PK and PA elements are well mixed and that there is not a significant difference in composition between the matrix and dispersed phases, implying that the interface thickness of the PK/PA blend is thicker than that of the PK/SAN blend. However, this may be because the lateral resolution of the line scanning in the measurement technique was insufficient to observe changes in composition.

The interface thickness measured in this study was found to be greater than 2–6 nm for PVC/PS, PS/PMMA, and PVC/SAN blends prepared by solvent casting [49], 50–80 nm for PA/polyolefin elasomer (POE) immiscible blends and maleic anhydride (POE-g-MAH) compatible blends estimated by nanoprobing AFM [52], and greater than about 100 nm for poly(L-lactic acid)/poly(vinylidene fluoride) immiscible blends investigated by STEM/EDX and electron energy loss spectroscopy (EELS) [53]. Liao et al. [54] measured the interface thickness of poly(methyl methacrylate) (PMMA)/SAN miscible pairs using energy-fitting TEM and showed that the interface thickness varies with temperature and time

during sheet lamination and can reach up to 700 nm. The Favis research group reported that the interfacial thickness of a PLA/PBS immiscible blend measured by ToF-SIMS was approximately 2 μm [31]. The interfacial thickness of the immiscible polymer blends in these studies is much larger than the value obtained in this study.

These results suggest that combining SEM morphological observation with EDS elemental line scanning can be a more advanced method for measuring interfacial thickness and evaluating the compatibility of polymer blends. Future advancements in EDS line scanning technology are expected to contribute significantly to the quantitative measurement of compatibility in the field of polymer blends.

Conclusions

In this study, comparative morphological observations of the PK/SAN blend and the PK/PA blend were performed using SEM-EDS mapping. For both the PK/SAN blend and the PK/PA blend, the SEM/EDS elemental mapping images showed a clearer contrast between the matrix and domain phases than the SEM images alone. In the case of the PK/SAN/additive blend, a domain-in-domain morphology and layered structure were observed using the SEM/EDS elemental mapping technique. These images were confirmed through comparison with TEM observation results.

In elemental line scanning mode, for the PK70/SAN30 blend, the intensity of oxygen elements exhibits a downward convex shape at the interface where the PK matrix and SAN domains intersect, whereas the intensity of nitrogen elements increases until reaching a flat region, then decreases as it passes through other interfaces. For the PK30/SAN70 blend, the line scanning profile shows a shape opposite to that of the PK70/SAN30 blend. In line scanning mode, when passing through the PA region of the PK70/PA30 blend, the intensity of oxygen elements is convex downward, while the intensity of nitrogen elements is convex upward.

The slope across the interface of the PK/SAN blend appeared steeper than that of the PK/PA blend. The interface thickness of the PK/SAN blend was estimated to be in the range of 0.17–0.51 μm for oxygen elements. In contrast, the interface thickness of the PK70/PA30 blend was estimated to be greater than 0.37–0.76 μm, and in the case of PK30/PA70, the change in slope was very small, making it difficult to distinguish the compositional difference between the two phases. As interdiffusion increases, the interface becomes too wide, making it difficult to distinguish. These results suggest that the PK/PA blend has higher compatibility compared to the PK/SAN blend. This suggests that combining SEM morphological observation with EDS elemental line scanning can be a more effective method for measuring interface thickness and evaluating the compatibility of polymer blends.

Declarations

The authors declare no Funding and/or Conflict of interest/Competing interests.

Funding:

No funding

Acknowledgements

The author would like to thank Researcher Youngho Eom of Cheil Industries for taking the TEM images and Researcher Hyunji Kwon of the National NanoFab Center for assisting with the SEM/EDS analysis.

References

1. Olabisi O, Robeson LM, Shaw MT (1979) Polymer–polymer miscibility. Academic, New York
2. Paul DR, Newman S (1978) Polymer blends. Academic, New York
3. Asano A, Nishioka M, Takahashi Y, Kato A, Hikasa S, Iwabuki H, Nagata K, Sato H, Hasegawa T, Sawabe H, Arao M, Suda T, Isoda A, Mukai M, Ishikawa D, Izumi T (2009) High impact properties of polyketone/polyamide-6 alloys induced by characteristic morphology and water absorption. Macromol 42:9506–9514
4. Kato A, Nishioka M, Takahashi Y, Suda T, Sawabe H, Isoda A, Drozdova O, Hasegawa T, Izumi T, Nagata K, Hikasa S, Iwabuki H, Asano A (2010) Phase separation and mechanical properties of polyketone/polyamide polymer Alloys. J Appl Polym Sci 116:3056–3069
5. Son Y, Lee S (2023) Compatibility between aliphatic polyketone terpolymer and nylon 6 polymer blend. J Polym Res 30:33
6. Lee HC, Son Y, Lee S (2019) Study of compatibility between aliphatic polyketone terpolymer and poly(styrene-r-acrylonitrile). J Appl Polym Sci 137:48743
7. Kwon HG, Hwang T, Kim DH, Son Y (2021) Study on the effect of chemical reaction between component polymers and gelation on the physical properties of aliphatic polyketone/polyamide 6 blends. Polym Korea 45:748–756
8. Kwon HG, Park J, Kim N, Lee S, Shim J, Lee M, Kim DH, Son Y (2023) High impact strength of aliphatic polyketone/polyamide 6 blends induced by a chemical reaction. J Elastomers Plast 55(4)
9. Kim Y, Bae JW, Lee CS, Kim S, Jung H, Jho JY (2015) Morphology and Mechanical Properties of Polyketone Blended with Polyamide and Ethylene-Octene Rubber. Macromol Res 23:971–976
10. Chatani Y, Takizawa T (1961) Crystal structure of polyketone (1:1 ethylene/carbon monoxide copolymer). J Polym Sci 55:811–819
11. Sommazzi A, Garbassi F (1997) Olefin–carbon monoxide copolymers. Prog Polym Sci 22:1547–1605
12. Garbassi F, Sommazzi A, Meda L, Mestroni G, Sciutto A (1998) Surface properties of aliphatic polyketone. Polymer 39:1503–1506

13. Waddon AJ, Karttunen NR, Lesser AJ (1999) On the crystalline structure and morphology of aliphatic ketone terpolymer. Macromolecules 32:423–428
14. Lagaron JM, Vickers ME, Powell AK (2002) Effect of the nature of the side chain on the crystalline structure in aliphatic polyketones. Polymer 43:1866–1877
15. Housung Corporation Catalogue and Technical bulletin
16. Shkolnik S, Weil ED (1988) Stabilization of alternating carbon monoxide–ethylene copolymer. J Appl Polym Sci 69:1691–1704
17. Chiantore O, Lazzari M, Ciardelli F, Vito SD (1997) Pyrolysis and thermal degradation of ethylene–carbon monoxide alternating copolymers. Macromolecules 30:2589–2597
18. Lommerts BJ (2001) Influence of catalyst remnants on thermal degradation during melt processing of ethylene–carbon monoxide copolymers. Polymer 42:6281–6287
19. Yang Y, Li SY, Bao RY, Liu ZY, Yang MB, Tan CB, Yang W (2018) Progress in polyketone materials: blends and composites. Polym Int 67:1418–1487
20. Zuiderduin WCJ, Homminga DS, Huétink J, Gaymans RJ (2003) Toughening of polypropylene with calcium carbonate particles. Polymer 44:6361–6370
21. Zuiderduin WCJ, Homminga DS, Huétink J, Gaymans RJ (2003) Influence of Copolymerisation on Fracture Behaviour of Aliphatic Polyketones. Polymer 46:1921–1934
22. Xu FY, Chien JCW (1994) Miscible polymer blends of propylene–carbon monoxide copolymer with poly(methyl methacrylate). Macromolecules 27:6589–6593
23. de Vos SC, Huhn W, Rieger B, Möller M (1999) Novel blends of alternating propene-carbon monoxide copolymers and styrenic copolymers. Polym Bull 42:611–618
24. Marklund E, Gedde UW, Hedenqvist MS, Wiberg G (2001) Properties of polyketone/polypropylene blends. Polymer 42:3153–3160
25. Lim MY, Kim HJ, Baek SJ, Kim KY, Lee SS, Lee JC (2014) Improved strength and toughness of polyketone composites using extremely small amount of polyamide 6 grafted graphene oxides. Carbon 77:366–378
26. Han S, Löhr SC, Baldermann A, Farkas J, McMahon W, Milliken KL, Rafiei M, Wheeler C, Owen M (2022) Earth system science applications of next-generation SEM-EDS automated mineral mapping. Front Earth Sci 10:956912
27. Moore KL, Lombi E, Zhao FJ, Grovenor CRM (2012) Elemental imaging at the nanoscale: NanoSIMS and complementary techniques for element localisation in plants. Anal Bioanal Chem 402:3263–3273
28. Kulawik K, Buffat PA, Kruk A, Wusatowska-Sarnek AM (2015) Imaging and characterization of γ' and γ" nanoparticles in Inconel 718 by EDX mapping. Mater Charact 100:74–80
29. Gupper A, Wilhelm P, Schmied M, Kazarian SG, Chan KLA, Reußner J (2002) Combined application of imaging methods for characterization of a polymer blend. Appl Spectrosc 56:1515–1523

30. Zorn G, Dave SR, Gao X, Castner DG (2011) Determining elemental composition in quantum dots. Anal Chem 83:866–873
31. Ravati S, Poulin S, Piyakis K, Favis BD (2014) Phase identification in ternary polymer blends by ToF-SIMS. Polymer 55:6110–6123
32. Chen CC, White JL (1993) Compatibilizing agents in polymer blends. Polym Eng Sci 33:923–930
33. Sémeril D, Passaglia E, Bianchini C, Davies M, Miller H, Ciardelli F (2003) Reactive Blending of Polyamides with Different Carbonyl Containing Olefin Polymers. Macromol Mater Eng 288:475–483
34. Oshinski AJ, Keskkula H, Paul DR (1992) Rubber toughening of polyamides with functionalized block copolymers: 1. Nylon-6. Polymer 33:268–283
35. Huang JJ, Paul DR (2006) Comparison of fracture behavior of nylon 6 versus an amorphous polyamide toughened with maleated poly(ethylene-1-octene) elastomers. Polymer 47:3505–3519
36. Macosko CW, Jeon HK, Hoye TR (2005) Reactions at polymer–polymer interfaces for compatibilization. Prog Polym Sci 30:939–947
37. Guégan P, Macosko CW, Ishizone T, Hirao A, Nakahama S (1994) Kinetics of chain coupling at melt interfaces. Macromolecules 27:4993–4994
38. Lee S, Park OO (2001) Preparation of compatibilizer via melt blending and application in PC/PS blends. Polymer 42:6661–6668
39. Kim SJ, Kim DK, Cho WJ, Ha CS (2003) Morphology and properties of PBT/nylon 6/EVA-g-MAH ternary blends prepared by reactive extrusion. Polym Eng Sci 43:1298–1311
40. Reis AV, Fajardo AR, Schuquel ITA, Guilherme MR, Vidotti GJ, Rubira AF, Muniz EC (2009) Reaction of Glycidyl Methacrylate at the hydroxyl and carboxylic groups of poly(vinyl alcohol) and poly(acrylic acid): Is this reaction mechanism still unclear? J Org Chem 74:3750–3757
41. Escriba-Flores AA, Fernandez-Francos X, Ferrando FF, Fabregat-Sanjuan A (2025) Tunable dual-curing acrylic/epoxy systems for 3D printing with enhanced joint performance via carbon nanotubes. Polymer 334:128768
42. Wang X, Mi J, Wang J, Zhou H (2018) Multiple actions of poly(ethylene octene) grafted with glycidyl methacrylate on the performance of poly(lactic acid). RSC Adv 8:34418–34427
43. Bednarczyk P, Mozelewska K, Nowak M, Czech Z (2021) Photocurable Epoxy Acrylate coatings preparation by dual cationic and radical photocrosslinking. Materials 14:4150
44. Yang Y, Li SY, Bao RY, Liu ZY, Yang MB, Tan CB, Yang W (2018) Progress in polyketone materials: blends and composites. Polym Int 67:1478–1487
45. Li S, Yang Y, Zha X, Zhou Y, Yang W, Yang M (2018) Nanoscale morphology, interfacial hydrogen bonding, confined crystallization and greatly improved toughness of polyamide12/polyketone blends. Nanomater 8:932
46. Lee J, Lee KH, Kim D, Lim S, Lee SS (2013) Layered nanofiller reinforced polketone composites. Macromol Res 21:1270–1273

47. Drouin D, Couture AR, Joly D, Tastet X, Aimez V, Gauvin CASINO R V2.42-A fast and easy-to-use modeling tool for scanning electron microscopy and microanalysis users. Scanning 29:92–101
48. Mura F, Cognigni F, Ferroni M, Morandi V, Rossi M (2023) Advances in Focused Ion Beam Tomography for Three-Dimensional Characterization in Materials Science. Materials 16:5808
49. Ramya P, Ranganathaiah C, Williams JF (2012) Experimental determination of interface widths in binary polymer blends from free volume measurements. Polymer 53:4539–4546
50. Kommri Y, Tanisuchi A, Shinbata H, Goto S, Saito H (2023) Phase-Separated Structure of NBR/PVC Blends with Different Acrylonitrile Contents Investigated Using STEM–EDS Mapping Analysis. Polymers 15:3343
51. ASTM E1438-11 (2019) Standard Guide for Measuring Widths of Interfaces in Sputter Depth Profiling Using SIMS. ASTM International
52. Li TT, Cheng SI, Feng LF, Gu XP, Zhang CL, Hu GH Measuring the Interfacial Thickness of Immiscible Polymer Blends by Nano-probing of Atomic Force Microscopy. Chinese J Polym Sci 40: 421–430 [53] Dong, Hakukawa W, Yamahira H, Li N, Horiuchi Y (2022) S (2019) Mechanism of Reactive Compatibilization of PLLA/PVDF Blends Investigated by Scanning Transmission Electron Microscopy with Energy-Dispersive X–ray Spectrometry and Electron Energy Loss Spectroscopy. ACS Appl Polym Mater 1:815–824
53. Liao Y, Nakagawa A, Horiuchi S, Ougizawa T (2007) Interdiffusion at Homopolymer/Random Copolymer Interfaces, Investigated by Energy-Filtering Transmission Electron Microscopy. Macromol 40:7966–7972

Figures

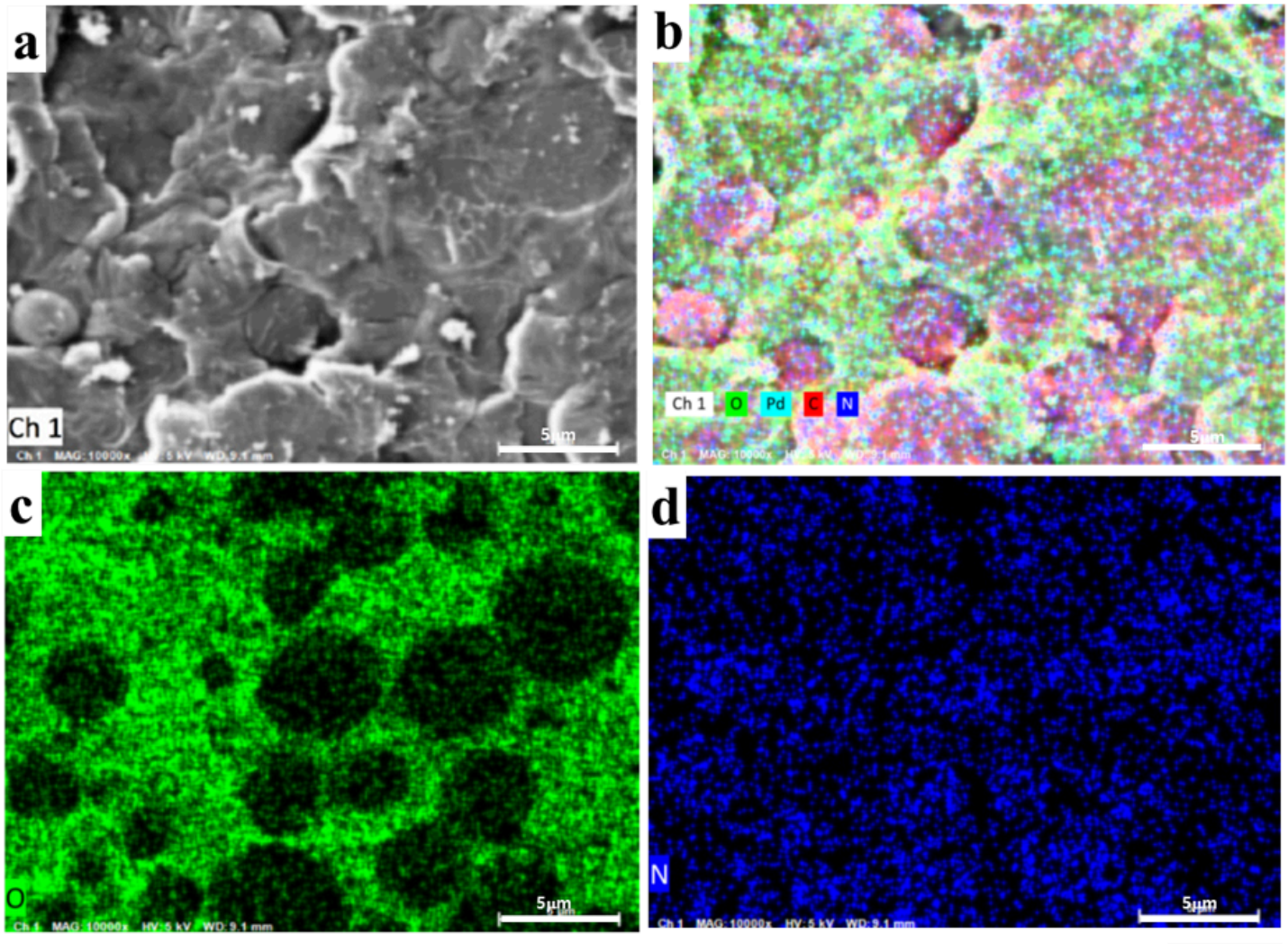


Figure 1

Morphological observations of PK70/SAN30 blends using a combination of SEM and EDS elemental mapping. a) SEM photograph, b) C, O, and N elements, c) O element, d) N element.

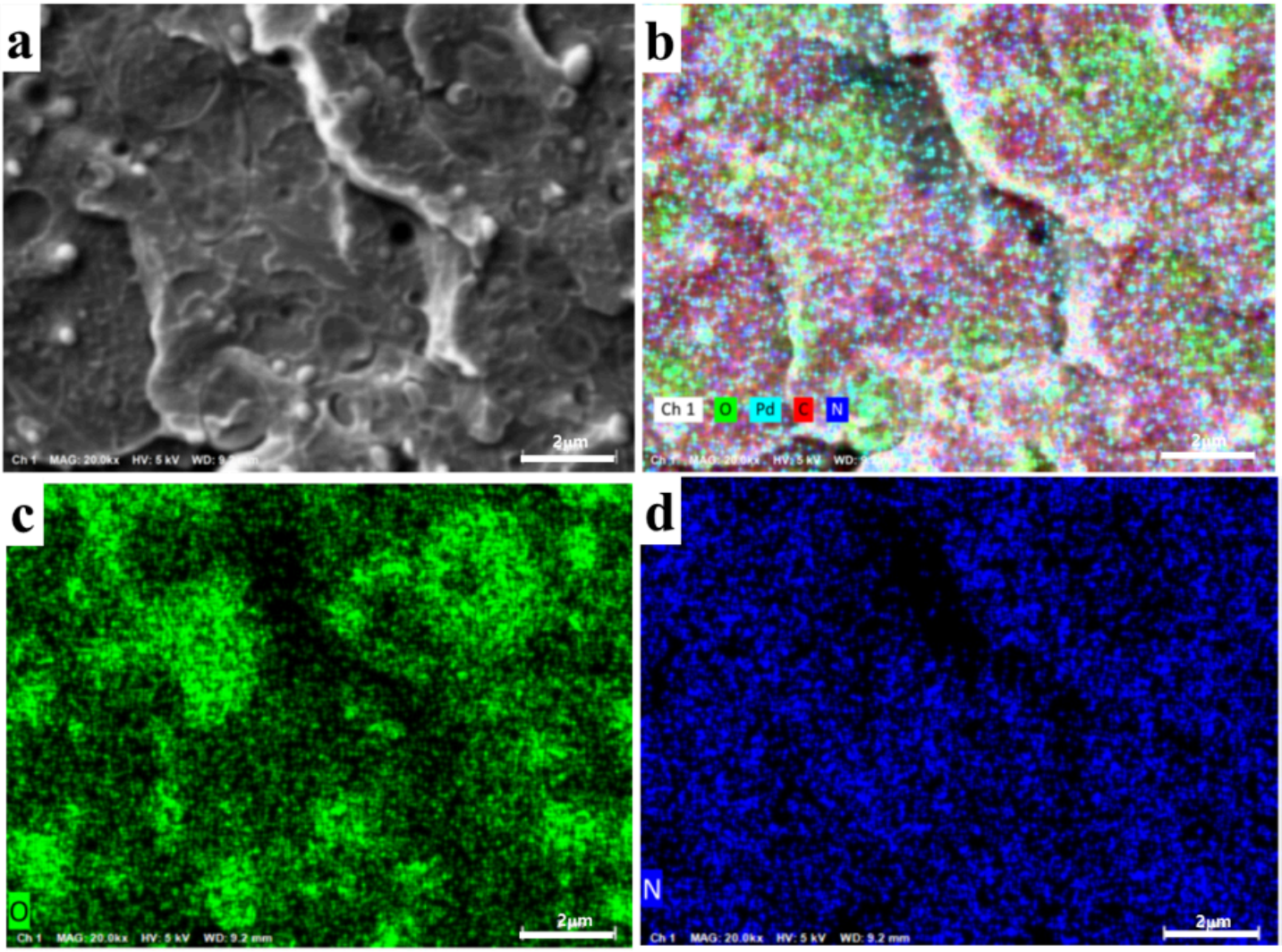


Figure 2

Morphological observations of PK30/SAN70 blends using a combination of SEM and EDS elemental mapping. a) SEM, b) C, O, and N elements, c) O element, d) N element.

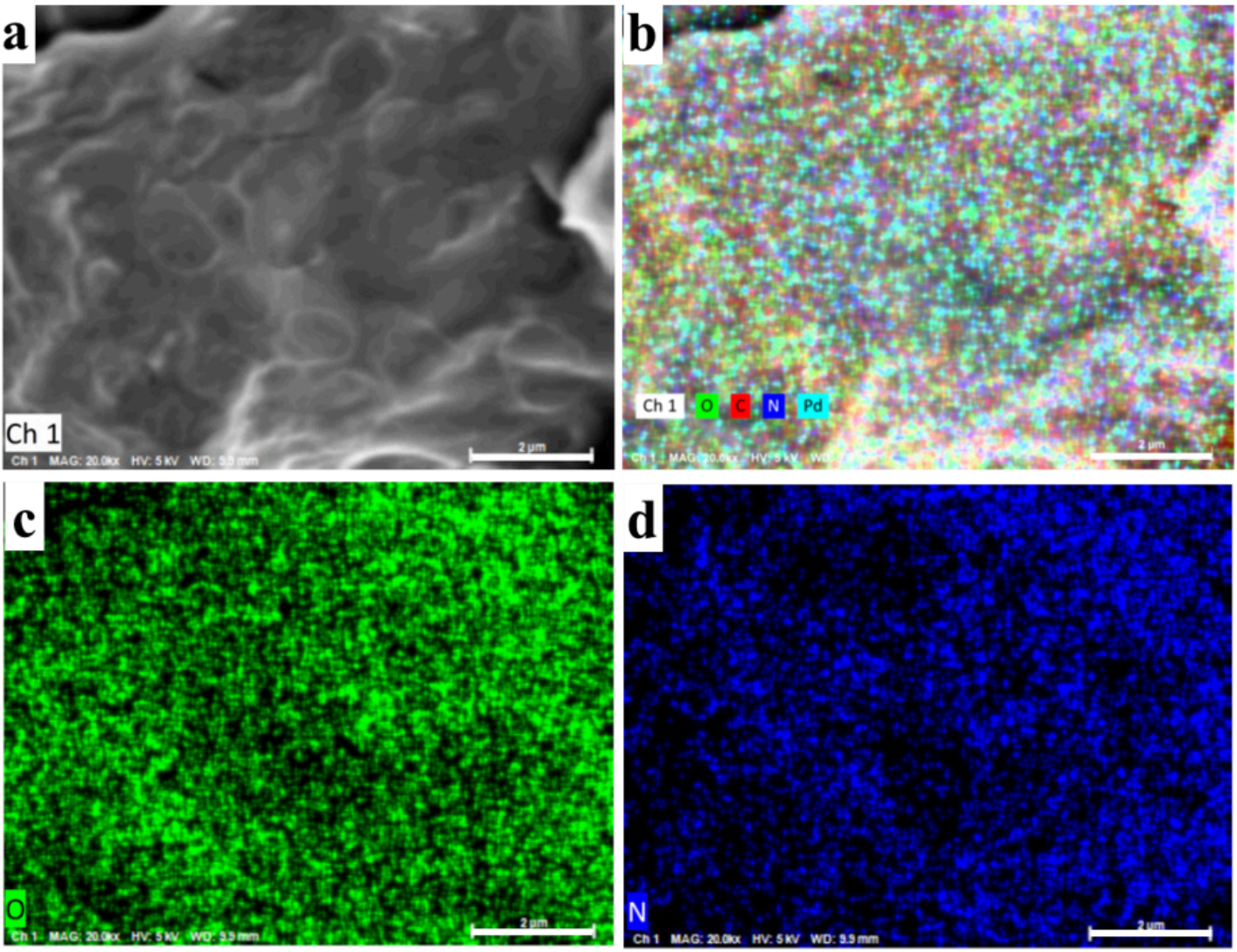


Figure 3

Morphological observations of PK70/PA30 blends using a combination of SEM and EDS elemental mapping. a) SEM, b) C, O, and N elements, c) O element, d) N element.

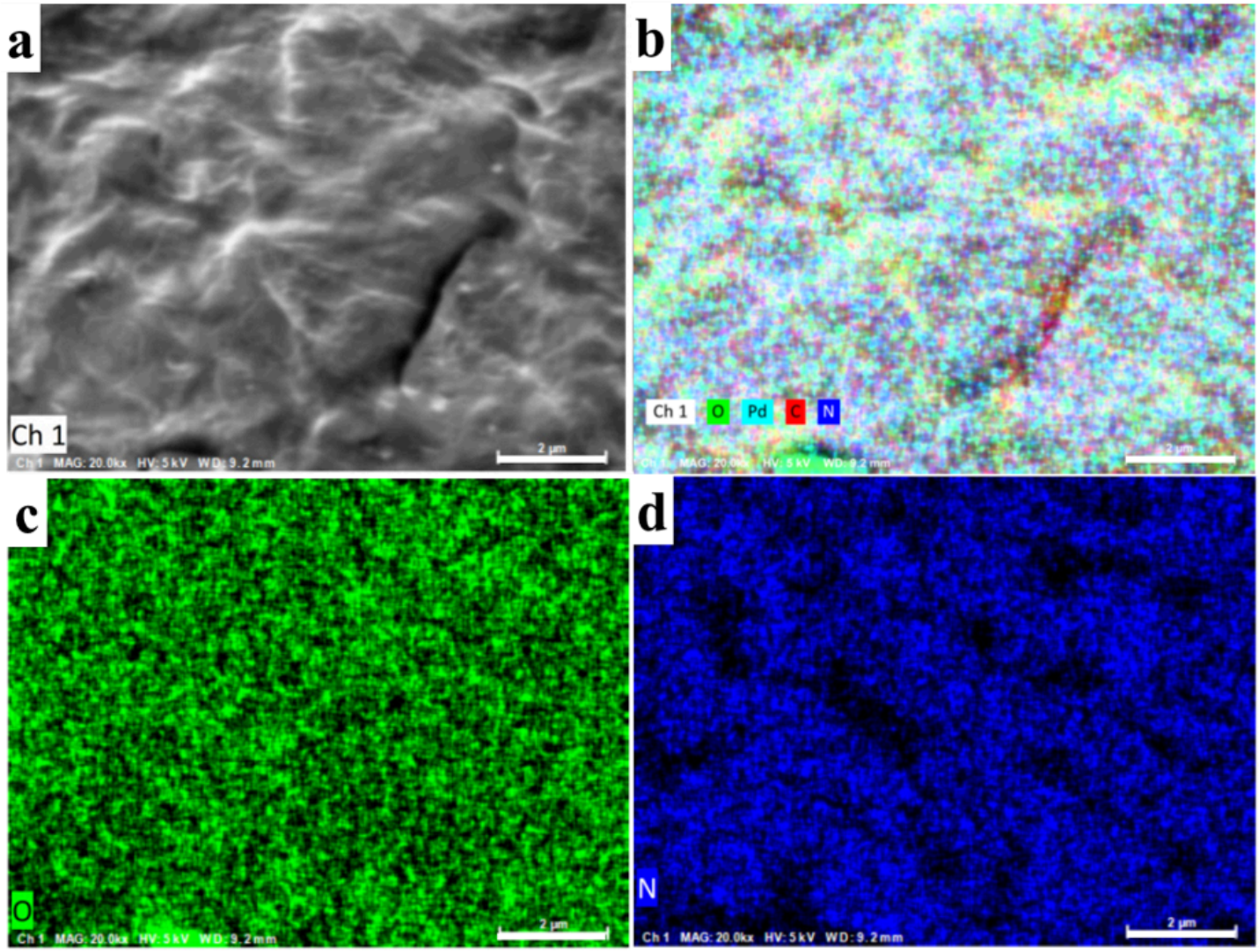


Figure 4

Morphological observations of PK30/PA70 blends using a combination of SEM and EDS elemental mapping. a) SEM, b) C, O, and N elements, c) O element, d) N element.

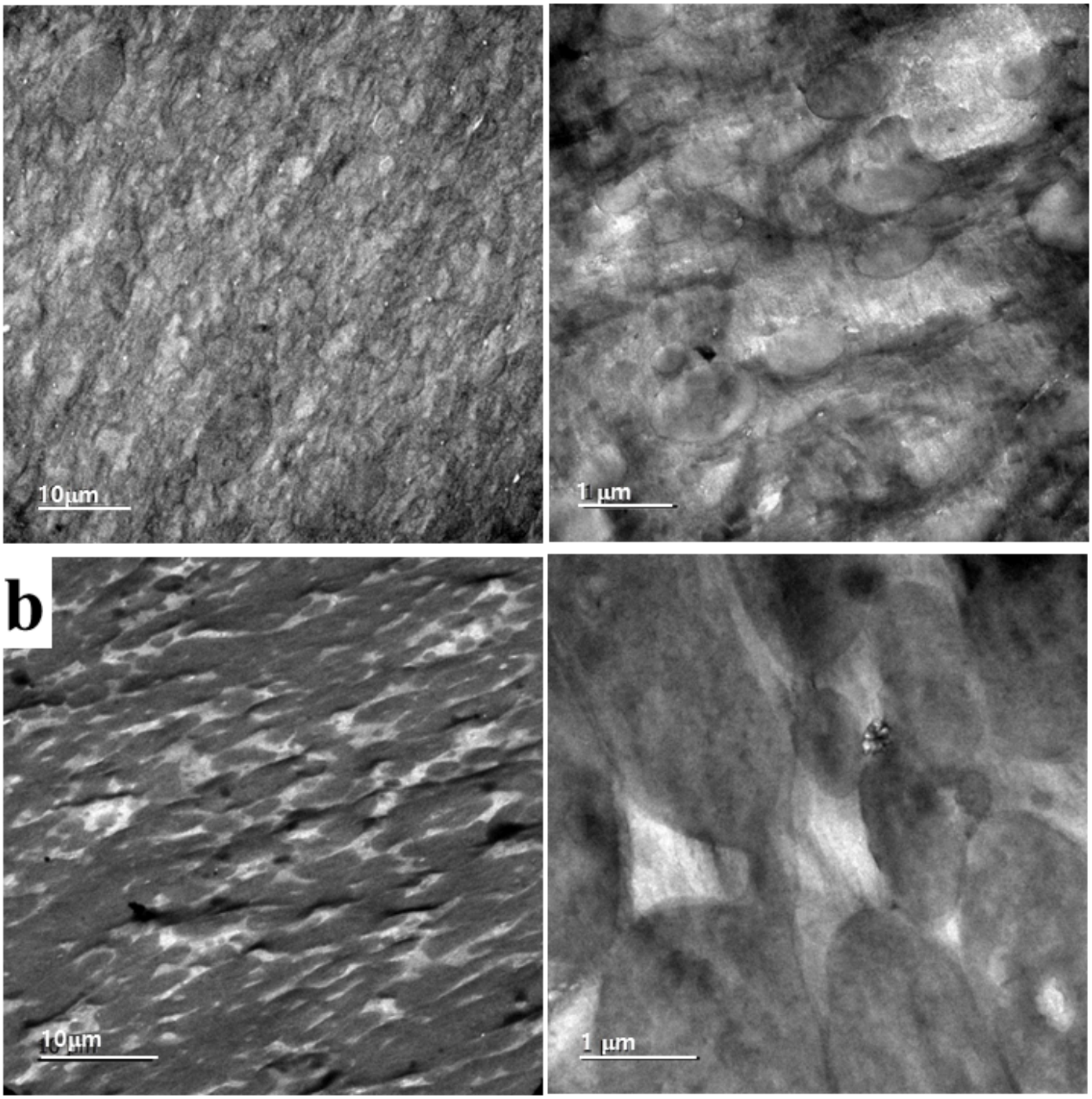


Figure 5

TEM observations after OsO_4 treatment following PTA staining. a) PK70/PA30 blend, b) PK30/PA70 blend.

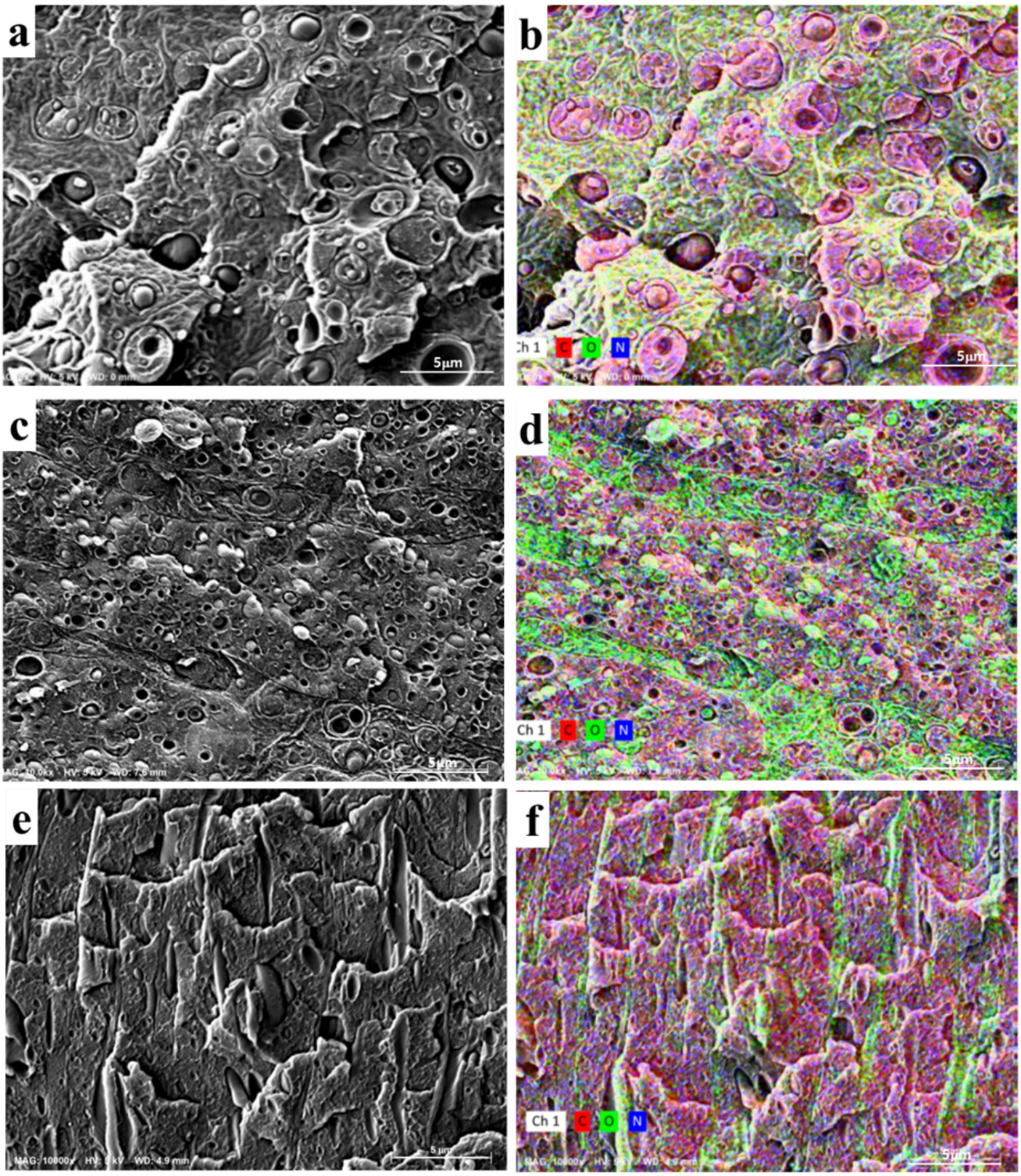


Figure 6

Observation of morphological changes in PK/SAN blends with added compatibilizers using SEM/EDS mapping mode. a) SEM image of the PK70/SAN25/additive5 blend in a direction perpendicular to the flow and b) EDS mapping, c) SEM image of PK25/SAN70/additive5 in a direction perpendicular to the flow and d) EDS mapping, e) SEM image of the PK25/SAN70/additive5 blend in the flow direction and f) EDS mapping.

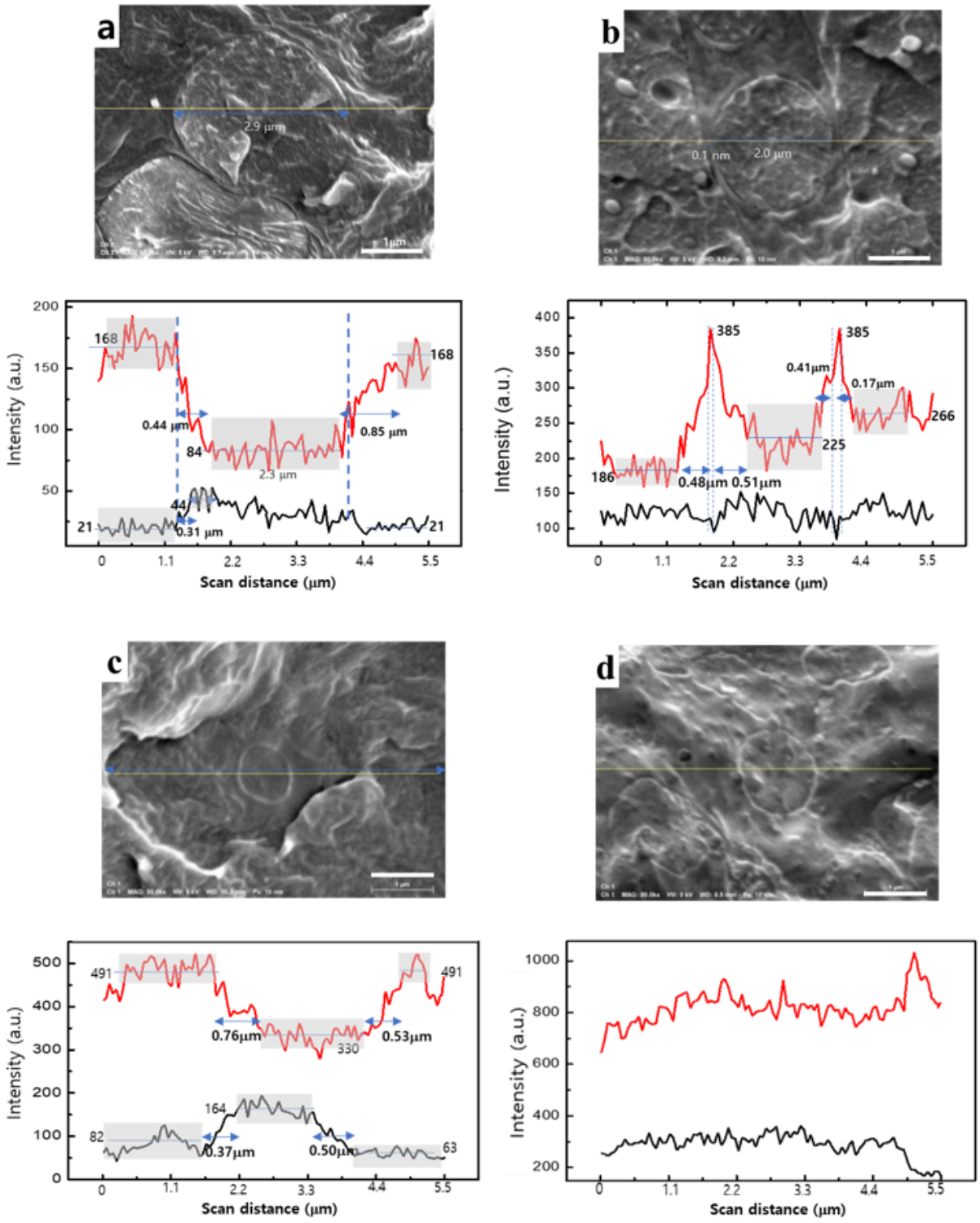


Figure 7

SEM image (top) and pulse intensity in SEM/EDS line scanning (bottom). a) PK70/SAN30 blend, b) PK30/SAN70 blend, c) PK70/PA30 blend, d) PK30/PA70 blend.

Supplementary Files

This is a list of supplementary files associated with this preprint. Click to download.

- supportinginformation.docx